Modelling Simul. Mater. Sci. Eng. 1 (1993) 569–590. Printed in the UK

Evolution dynamics of 3D periodic microstructures in irradiated materials

N M Ghoniem and D Walgraef†

Mechanical, Aerospace and Nuclear Engineering Department, UCLA, Los Angeles, CA 90024, USA

Received 27 May 1992, accepted for publication 21 March 1993

Abstract. The formation and evolution of defect microstructures in irradiated materials is analysed in the framework of a dynamical model for the evolution of the two fundamental defects of irradiated microstructures, namely vacancy and interstitial clusters. The effects of irradiation on materials is described by dynamical equations for two mobile atomic size species (vacancies and interstitial atoms), and two basic immobile elements of the microstructure (vacancy and interstitial clusters). It is shown that uniform vacancy and interstitial loop distributions may become unstable during irradiation and that they will form large-scale spatially organized distributions, in a specific range of irradiation and material conditions. The selection and stability of the resulting microstructures are studied in the quasi-static approximation and in the weakly non-linear regime around the bifurcation point. It is shown that, after transients corresponding to three-dimensional BCC patterns, the final pattern should correspond to planar wall structures in agreement with experimental observations.

1. Introduction

Many irradiated materials present several types of microstructures which correspond to the spatial organization of defect populations. Well-known examples are void [1–3] and bubble lattices [4–6], precipitate ordering [7], defect walls and vacancy loop ordering [8–10]. In particular, the spatial ordering of vacancy dislocation loops occurs frequently in metals and alloys irradiated at moderate doses and high temperatures [11]. The uniform distribution of loops which are created by the collapse of cascades becomes unstable beyond some threshold which is determined by various material and irradiation parameters (e.g., the irradiation dose, damage rate, bias in the migration of point defects to loops and network dislocations, and temperature). In a preceding study [12], we analysed a simplified model proposed by Murphy [13] to describe the dynamics of defect populations in metals and alloys under particle irradiation. This model is based on the rate theory of radiation damage originally developed by Bullough and co-workers [14], and expanded further by Ghoniem and Kulcinski [15] to include the dynamics of point defects in the fully dynamic rate theory.

In the models analysed by Murphy [13], and by Walgraef and Ghoniem [12], network dislocations are assumed to have a constant uniform distribution. Furthermore, the effect of interstitial loop formation is not taken into account and the interstitial loop density is considered as a part of the network density. By considering the basic elements of defect

† Director of Research at the Belgian National Fund for Scientific Research. Permanent address: Service de Chimie Physique and Center for Nonlinear Phenomena and Complex Systems, Free University of Brussels, CP 231, B-1050 Brussels, Belgium.

0965-0393/93/050569+22$07.50

dynamics; namely point defect creation, recombination and migration to microstructures, the kinetic equations for defect concentrations are obtained. It was shown by us that a pattern-forming instability occurs at a critical value of the mean vacancy loop density and a critical wavelength. In the sink dominated regime, the corresponding threshold can be expressed as a function of material and irradiation parameters. We showed that instability occurs when the uniform vacancy loop density exceeds the network density multiplied by a function of the bias B and of the cascade collapse efficiency ϵ (i.e. $\rho_L > \rho_N/(\sqrt{B/\epsilon}-1)^2$). Furthermore, the critical wavelength decreases with increasing network dislocation density, cascade collapse efficiency and damage rate. Experimental verifications of these findings were discussed in our earlier work [12].

Since the linear analysis only determines the wavelength of the ordered microstructure that is expected to develop beyond the instability point, but not its symmetry, a non-linear analysis in the post-bifurcation regime is needed to discuss the selection and stability of emerging patterns. Hence, we performed the weakly non-linear analysis of the problem by deriving amplitude equations for the microstructures [12]. In the systems considered here, the spatial fluctuations of vacancy and interstitial concentrations evolve much more rapidly than vacancy loop density fluctuations. In such a situation the dynamics can be reduced, through a multiple scale analysis [16] or via an adiabatic elimination of the fast variables [17], to the dynamics of the slow mode or order parameter-like variable which is proportional to the deviations of the loop density from its uniform value. In our earlier analysis we showed that the stable patterns correspond to:

(i) roll or wall structures associated with spatial modulations of the vacancy loop density in one direction. They appear via a second-order-like transition, or a supercritical bifurcation;

(ii) rodlike hexagonal or triangular structures appearing via a first-order-like transition (subcritical bifurcations);

(iii) BCC lattices or filamental structures of cubic symmetry, also associated with a subcritical bifurcation and defined similarly to hexagonal structures but with six pairs of wavevectors.

Hence one sees that, on increasing the bifurcation parameter (e.g. the mean loop density), one should expect a transition from a uniform distribution to BCC and finally to wall structures. However, this analysis was performed by neglecting the time evolution of the interstitial loop density, which may prevent the system from following the path anticipated on the basis of the evolution of vacancy loop density alone.

The aim of the present work is to formulate and analyse a dynamical model which considers the two major elements of irradiated microstructures, namely vacancy and interstitial clusters. In this regard, we model the effects of irradiation on materials in the form of dynamical equations for two mobile atomic-size species (vacancies and interstitial atoms), and two basic immobile elements of the microstructure (vacancy and interstitial clusters).

2. The dynamical model

In order to explicitly account for the effect of interstitial loops on the evolution of defect populations, we propose the following dynamical model, which is based on two point-defect equations including spatial diffusion operators and a set of equations describing the

evolution of loops (this model is obtained from a more detailed analysis of the kinetics of interstitial loop formation, and is given in Appendix A):

$$\begin{aligned}
\partial_t c_\mathrm{i} &= K - \alpha c_\mathrm{i} c_\mathrm{v} + D_\mathrm{i}\nabla^2 c_\mathrm{i} - D_\mathrm{i} c_\mathrm{i}(Z_{\mathrm{i}N}\rho_N + Z_{\mathrm{i}\mathrm{V}}\rho_\mathrm{V} + Z_{\mathrm{i}\mathrm{I}}\rho_\mathrm{I}) \\
\partial_t c_\mathrm{v} &= K(1-\epsilon) - \alpha c_\mathrm{i} c_\mathrm{v} + D_\mathrm{v}\nabla^2 c_\mathrm{v} - D_\mathrm{v}\big(Z_{\mathrm{v}N}(c_\mathrm{v} - \bar{c}_{\mathrm{v}N})\rho_N \\
&\qquad + Z_{\mathrm{v}\mathrm{V}}(c_\mathrm{v} - \bar{c}_{\mathrm{v}\mathrm{V}})\rho_\mathrm{V} + Z_{\mathrm{v}I}(c_\mathrm{v} - \bar{c}_{\mathrm{v}I})\rho_\mathrm{I}\big) \\
\partial_t \rho_\mathrm{I} &= (2\pi N/|b|)\big(D_\mathrm{i} Z_{\mathrm{i}\mathrm{I}} c_\mathrm{i} - D_\mathrm{v} Z_{\mathrm{v}I}(c_\mathrm{v} - \bar{c}_{\mathrm{v}I})\big) \\
\partial_t \rho_\mathrm{V} &= \Big(1/|b| r_V^0\Big)\big[\epsilon K - \rho_\mathrm{V}(D_\mathrm{i} Z_{\mathrm{i}\mathrm{V}} c_\mathrm{i} - D_\mathrm{v} Z_{\mathrm{v}\mathrm{V}}(c_\mathrm{v} - \bar{c}_{\mathrm{v}\mathrm{V}}))\big]
\end{aligned} \tag{1}$$

where c_v corresponds to vacancies and c_i to interstitials. ρ_N is the network dislocation density, ρ_V the vacancy loop and ρ_I the interstitial loop density. K is the displacement damage rate and ϵ the cascade collapse efficiency, α is the recombination coefficient, b the Burgers vector, r_V^0 the mean vacancy loop radius and $Z_{\ldots}$ are the bias factors which will be approximated by $Z_{\mathrm{i}N} = 1 + B$, $Z_{\mathrm{i}\mathrm{I}} \cong Z_{\mathrm{i}\mathrm{V}} = 1 + B'$ and $Z_{\mathrm{v}\mathrm{I}} = Z_{\mathrm{v}N} = Z_{\mathrm{v}\mathrm{V}} = 1$. B is the excess network bias and B' is the excess loop bias ($B' > B$). $\bar{c}_{\mathrm{v}N}$, $\bar{c}_{\mathrm{v}\mathrm{V}}$ and $\bar{c}_{\mathrm{v}\mathrm{I}}$ are the concentrations of thermally emitted vacancies from network dislocations, vacancy and interstitial loops, respectively.

We shall now use the following scaling relations:

$$\begin{aligned}
&\lambda_\mathrm{v} = D_\mathrm{v} Z_{\mathrm{v}N}\rho_N \qquad \bar{D}_\cdot = D_\cdot/\lambda_\mathrm{v} \qquad \alpha/\lambda_\mathrm{v} = \gamma \qquad P = \gamma K/\lambda_\mathrm{v} \\
&\rho^*_{v,I} = \rho_{\mathrm{v},\mathrm{I}}/\rho_N \qquad x_{i,v} = \gamma c_{i,v} \qquad \bar{x}_{\mathrm{v}\mathrm{V}} \simeq \bar{x}_{\mathrm{v}\mathrm{I}} = \bar{x}_{\mathrm{v}L} \\
&\mu = Z_{\mathrm{i}N} D_\mathrm{i}/Z_{\mathrm{v}N} D_\mathrm{v} = (1+B) D_\mathrm{i}/D_\mathrm{v} \qquad \tau_V = b r_\mathrm{v}^0 \rho_N \gamma \qquad \tau = \lambda_\mathrm{v} t \\
&\tau_I = b\alpha\rho_N/2\pi N D_\mathrm{v}.
\end{aligned} \tag{2}$$

It is to be noted that while τ_V is constant, τ_I is dose dependent through the ρ_I^* term. Equation (1) can now be written in dimensionless form.

$$\begin{aligned}
\partial_\tau x_\mathrm{i} &= P - x_\mathrm{i} x_\mathrm{v} + \bar{D}_\mathrm{i}\nabla^2 x_\mathrm{i} - \mu x_\mathrm{i}(1 + \rho_\mathrm{V}^* + \rho_\mathrm{I}^*) \\
\partial_\tau x_\mathrm{v} &= P(1-\epsilon) - x_\mathrm{i} x_\mathrm{v} + \bar{D}_\mathrm{v}\nabla^2 x_\mathrm{v} - (x_\mathrm{v} - \bar{x}_{\mathrm{v}N}) - (x_\mathrm{v} - \bar{x}_{\mathrm{v}L})\rho_\mathrm{V}^* - (x_\mathrm{v} - \bar{x}_{\mathrm{v}L})\rho_\mathrm{I}^* \\
\tau_I \partial_\tau \rho_\mathrm{I}^* &= [\mu(1 + \Delta B) x_\mathrm{i} - (x_\mathrm{v} - \bar{x}_{\mathrm{v}L})] \\
\tau_V \partial_\tau \rho_\mathrm{V}^* &= \epsilon P - \rho_\mathrm{V}^*\big(\mu(1 + \Delta B) x_\mathrm{i} - (x_\mathrm{v} - \bar{x}_{\mathrm{v}L})\big).
\end{aligned} \tag{3}$$

To derive equation (3) from equation (1), we used the approximation: $B' \simeq B$ in point defect equations, and $(1 + B')/(1 + B) \simeq 1 + B' - B - BB' \simeq 1 + \Delta B$ in the interstitial loop equation, where ΔB is the difference between the loop and network bias. In order to gain analytical insight into the problem, we will consider here the case of a sink dominated regime. We will therefore ignore the effects of mutual point defect recombination. This can be viewed as the practical case of high temperature irradiated structural alloys. Generally, structural alloys are heavily cold-worked, and recombination effects are negligible. Ghoniem and Abromeit, however, have recently considered the effects of point defect irradiated microstructures [18]. Our intent here is to establish the conditions for the linear stability of the uniform dislocation loop densities (section 3), and then proceed to perform a stability analysis in the weakly non-linear regime (section 4) in order to determine the symmetries of the evolving microstructures. Since the point defect densities evolve much more rapidly than the loops, they may be adiabatically eliminated from the dynamics and their evolution related to that of the loop densities via the following relations:

$$x_\mathrm{v}^0 - \bar{x}_{\mathrm{v}L} = \frac{P(1-\epsilon) - \Delta}{1 + \rho_V^0 + \rho_I^0} \qquad x_\mathrm{i}^0 = \frac{P}{\mu(1 + \rho_V^0 + \rho_I^0)} \tag{4}$$

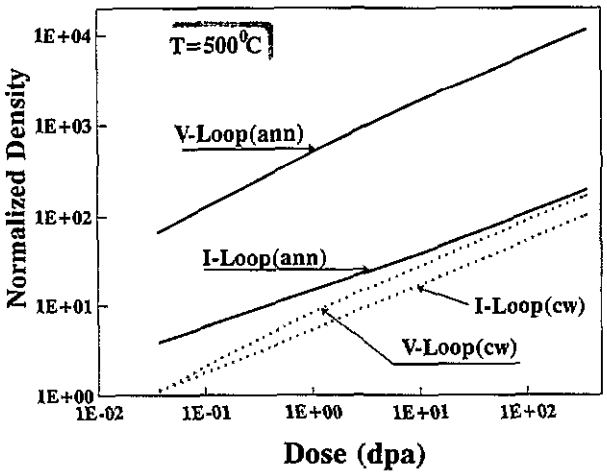

Figure 1. Normalized dislocation densities of vacancy (ρ_V^0) and interstitial (ρ_I^0) loops as a function of dose for typical reactor conditions (i.e. $K = 10^{-6}$ dpa s^{-1} and $T = 500$ °C). The network dislocation density is 10^{13} m^{-2} for annealed steels and 10^{15} m^{-2} for cold worked steels.

where $\Delta = \bar{x}_{vL} - \bar{x}_{vN}$.

The resulting reduced loop dynamics are approximately given by:

$$\partial_\tau \rho_I^0 = \frac{1}{\tau_I}\left(\frac{P(\epsilon + \Delta B) + \Delta}{1 + \rho_V^0 + \rho_I^0}\right) \qquad \partial_\tau \rho_V^0 = \frac{1}{\tau_V}\left(\epsilon P - \frac{\epsilon P + \Delta}{1 + \rho_V^0 + \rho_I^0}\rho_V^0\right). \tag{5}$$

We will now define a relaxation parameter, α, given by

$$\alpha = \left(\frac{\Delta + P\Delta B}{P(\epsilon + \Delta B) + \Delta}\right)\frac{\tau_I}{\tau_V} = \left(\frac{\Delta + P\Delta B}{P(\epsilon + \Delta B) + \Delta}\right)\frac{\rho_N}{N r_V^0}.$$

For typical material and irradiation conditions (i.e., $\rho_N = 10^{10}$ cm^{-2}, $N = 10^{15}$ cm^{-3}, $r_V^0 = 1.5 \times 10^{-7}$ cm) α is generally much larger than unity. The relationship between the vacancy and interstitial loop densities can easily be obtained from equation (5). This is given by

$$\rho_V^0 = \left[\epsilon P/(\Delta + P\Delta B)\right]\left\{\left(1 - 1/\alpha\right) + \rho_I^0 - \left(1 - 1/\alpha\right)e^{-\alpha\rho_I^0}\right\}. \tag{6}$$

Since α is shown to be generally greater than unity, and after a dose allowing ρ_I^0 to be greater than unity (i.e. interstitial loop dislocation density of the order of the network density), the transient term can be neglected, and the relationship can be cast in the simpler form:

$$\rho_V^0 \cong \left[\epsilon/\left(\epsilon' - \epsilon\right)\right](1 + \rho_I^0)$$

where we defined $\epsilon' = \Delta B + \Delta/P + \epsilon$

The time dependence of ρ_I^0 and ρ_V^0 is therefore given by:

$$\rho_I^0 = \sqrt{1 + \eta\tau} - 1 \qquad \rho_V^0 = \left[\epsilon/(\epsilon' - \epsilon)\right]\sqrt{1 + \eta\tau} \tag{7}$$

where $\eta = 2(P\Delta B + \Delta)/\tau_I = 4\pi(P\Delta B + \Delta)N D_v/B\rho_N\alpha$.

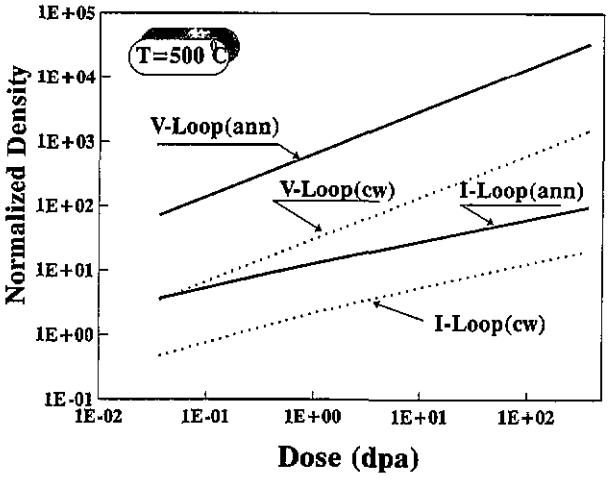

Figure 2. Normalized dislocation densities of vacancy (ρ_V^0) and interstitial (ρ_I^0) loops as a function of dose for typical low temperature accelerator conditions (i.e. $K = 10^{-3}$ dpa s^{-1} and $T = 500$ °C). The network dislocation density is 10^{13} m^{-2} for annealed steels and 10^{15} m^{-2} for cold worked steels.

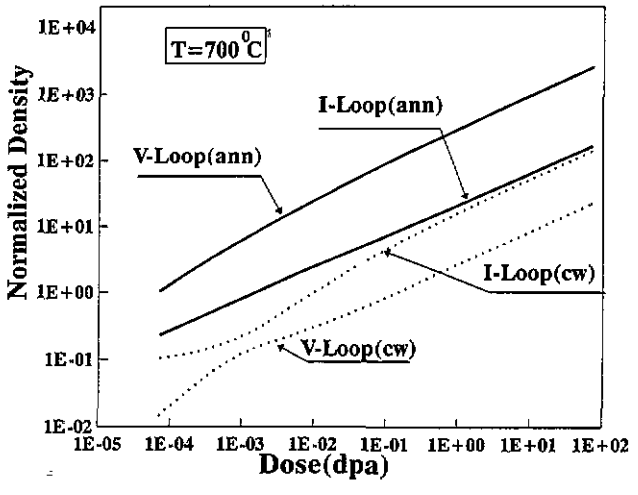

Figure 3. Normalized dislocation densities of vacancy (ρ_V^0) and interstitial (ρ_I^0) loops as a function of dose for typical high temperature accelerator conditions (i.e. $K = 10^{-3}$ dpa s^{-1} and $T = 700$ °C). The network dislocation density is 10^{13} m^{-2} for annealed steels and 10^{15} m^{-2} for cold worked steels.

It is clearly seen from this analysis that the quasi-steady-state dislocation densities for clustered defects will follow a $\sqrt{\tau}$ time dependence, after transients related to either interstitial loop nucleation, or to differences in the time constants of the two types of clusters. The dose dependence of ρ_i^0 and ρ_V^0 is illustrated in figures 1–3 for 316 stainless steel in various irradiation conditions. The relevant material and irradiation parameters are given in table 1.

Table 1. Material parameters for 316 stainless steels.

Parameter	Symbol	Value	Units
Vacancy formation energy	E_v^f	1.6	eV
Vacancy migration energy	E_v^m	1.3	eV
Interstitial migration energy	E_i^m	0.2	eV
Interstitial formation energy	E_i^f	4.0	eV
Vacancy diffusion (pre-exponential factor)	D_v^0	0.6	$cm^2\ s^{-1}$
Interstitial diffusion (pre-exponential factor)	D_i^0	10^{-3}	$cm^2\ s^{-1}$
Stacking fault energy	γ_{sf}	9.4×10^{12}	$eV\ cm^{-2}$
Shear modulus	$\mu/(1-\nu)$	4×10^{11}	dyne cm^{-2}
Burgers vector	b	2.5×10^{-8}	cm
Network bias excess	B	0.1	—
Loop/network bias excess	ΔB	0.05	—
Initial vacancy loop radius	r_V^0	1.5×10^{-7}	cm
Network dislocation density	ρ_N	$10^9 \times 10^{11}$	cm^{-2}
Displacement damage rate	K	10^{-6}–10^{-3}	dpa s^{-1}
Cascade collapse efficiency	ϵ	0.01–0.1	cm^{-3}
Interstitial loops number density	N	10^{14}–10^{16}	cm^{-3}

3. Linear stability of the uniform density

In order to check the possibility of pattern formation in our model, we perform the linear stability analysis of the uniform defect densities. This procedure consists of determining the linear evolution of the inhomogeneous perturbations of the uniform state. The occurrence of an instability would lead to the growth of such perturbations which are defined as:

$$\delta x_i = x_i - x_i^0 \qquad \delta x_v = x_i - (x_v^0 - \bar{x}_{vL})$$
$$\delta\rho_V = (\rho_V^* - \rho_V^0)/\rho_V^0 \qquad \delta\rho_I = (\rho_I^* - \rho_I^0)/\rho_I^0. \tag{8}$$

Introducing these variables in the system (3), we obtain the following equations for the Fourier components (wave vector, q) of point-defect perturbations (the equations are still within the approximation of fast point-defect evolution in the sink dominated regime):

$$\delta x_{iq} = -\frac{1}{\mu(1+\rho_V^0+\rho_I^0)+q^2\bar{D}_i}\left(\frac{P}{1+\rho_V^0+\rho_I^0}(\rho_V^0\delta\rho_{Vq}+\rho_I^0\delta\rho_{Iq}) + \int dk\ \mu\delta x_{ik}(\rho_V^0\delta\rho_{Vq-k}+\rho_i^0\delta\rho_{Iq-k})\right)$$
$$\delta x_{vq} = -\frac{1}{1+\rho_V^0+\rho_I^0+q^2\bar{D}_v}\left(\frac{\bar{P}}{1+\rho_V^0+\rho_I^0}(\rho_V^0\delta\rho_{Vq}+\rho_I^0\delta\rho_{Iq}) + \int dk\ \delta x_{vk}(\rho_V^0\delta\rho_{Vq-k}+\rho_I^0\delta\rho_{Iq-k})\right) \tag{9}$$

and its linear part may be written as:

$$\delta x_{iq} = -(\rho_V^0\delta\rho_{Vq}+\rho_I^0\delta\rho_{Iq})(P/\mu A_{Iq}A_0)$$
$$\delta x_{vq} = -(\rho_V^0\delta\rho_{Vq}+\rho_I^0\delta\rho_{Iq})(\bar{P}/A_{Vq}A_0) \tag{10}$$

where $A_0 = 1+\rho_V^0+\rho_I^0$, $A_{Vq} = A_0+q^2\bar{D}_v$, $A_{Iq} = A_0+q^2\bar{D}_v/(1+B)$ and $\bar{P} = P(1-\epsilon)-\Delta$.

The linear evolution of loop density perturbations is then given by:

$$\begin{aligned}\tau_V\partial_\tau\delta\rho_{vq} &= -\left(\epsilon P/\rho_V^0\right)\delta\rho_{vq} - \left[\mu(1+\Delta B)\delta x_{iq} - \delta x_{vq}\right] \\ \tau_I\partial_\tau\delta\rho_{Iq} &= \left[\mu(1+\Delta B)x_i^0 - (x_v^0 - \bar{x}_{vL})\right]\delta\rho_{Iq}/\rho_I^0 + \left[\mu(1+\Delta B)\delta x_{iq} - \delta x_{vq}\right]1/\rho_I^0\end{aligned} \tag{11}$$

or

$$\begin{aligned}\tau_V\partial_\tau\delta\rho_{Vq} &= -\left[\epsilon P/\rho_V^0 - \rho_V^0\Gamma_{IV,q}\right]\delta\rho_{vq} + \rho_I^0\Gamma_{IV,q}\delta\rho_{Iq} \\ \tau_I\partial_\tau\delta\rho_{Iq} &= -\left(\rho_V^0/\rho_I^0\right)\Gamma_{IV,q}\delta\rho_{vq} - \left[\Gamma_{IV,q} + (\epsilon P+\Delta)/A_0\rho_I^0\right]\delta\rho_{Iq}\end{aligned} \tag{12}$$

where

$$\Gamma_{IV,q} = P(1+\Delta B)/A_{Iq}A_0 - \bar{P}/A_{Vq}A_0 \tag{13}$$

The elements of the corresponding evolution matrix are time dependent. This situation prevents us from performing the usual stability analysis. However, some insight into the behavior of the system may be obtained within the quasi-static approximation, i.e. when the stability of the uniform densities is evaluated by considering them as frozen or stationary at each moment. One thus expects an instability when at least one eigenvalue of the evolution matrix acquires a positive real part. Of course this approximation does not describe correctly the growth rate of the perturbations, but in similar problems it seems to predict the instability threshold quite accurately [19]. Since it may be shown (cf Appendix B) that, in the vacancy loop dominated regime, one eigenvalue of the linear evolution matrix becomes positive when

$$(\rho_V^0)^2\Gamma_{IV,q} \geqslant \epsilon P \tag{14}$$

one expects, in this case, an instability threshold defined by

$$\left(\rho_V^0/A_0\right)\Big|_c = 2\sqrt{\epsilon B}/\left(B+\epsilon'\right) \tag{15}$$

$$q_c^2 = \rho_{vc}^0\sqrt{1+B}/2\sqrt{\epsilon/B}. \tag{16}$$

We will define the ratio ρ_V^0/A_0 as an appropriate bifurcation parameter for this problem. The bifurcation parameter, b, is then:

$$b \equiv \rho_V^0/A_0 = \rho_V^0/\left(1+\rho_V^0+\rho_I^0\right) \tag{17}$$

when b reaches its critical value, b_c, defined by (15), spatial instability in the vacancy loop population sets in. The evolution of the bifurcation parameter, b, as a function of dose, is shown in figure 4 for typical reactor conditions (i.e. $K = 10^{-6}$ dpa s^{-1} and T = 500 °C) for both cold worked and annealed steels. It is shown that the critical state for spatial instability in the vacancy loop population is reached only for annealed steels. The initial high network density of cold worked steels would suppress the transition to spatially ordered microstructures. The critical dose for annealed steels is shown to be very small, on the order of 10^{-3} dpa. Similar results are obtained for higher displacement rates, as in accelerator conditions at higher temperatures ($\simeq$ 700 °C) . At lower temperatures ($\simeq$ 500 °C) and under accelerator damage conditions, the transition from uniform to spatially

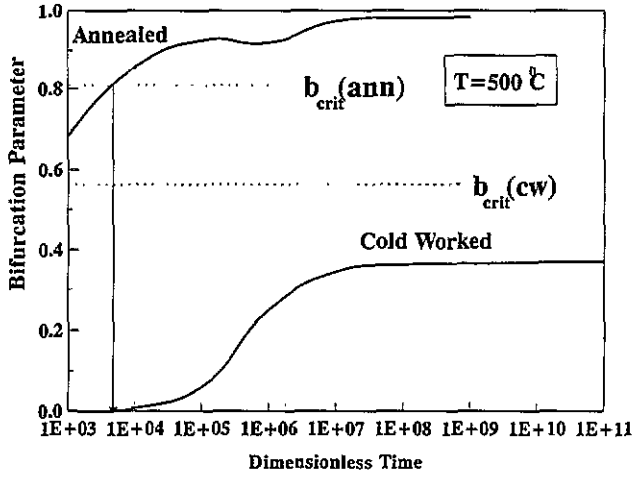

Figure 4. Evolution of the bifurcation parameter with irradiation dose for cold worked and annealed steel irradiated in typical reactor conditions (i.e. $K = 10^{-6}$ dpa s^{-1} and $T = 500$ °C). The dashed lines represent the critical values of the bifurcation parameter.

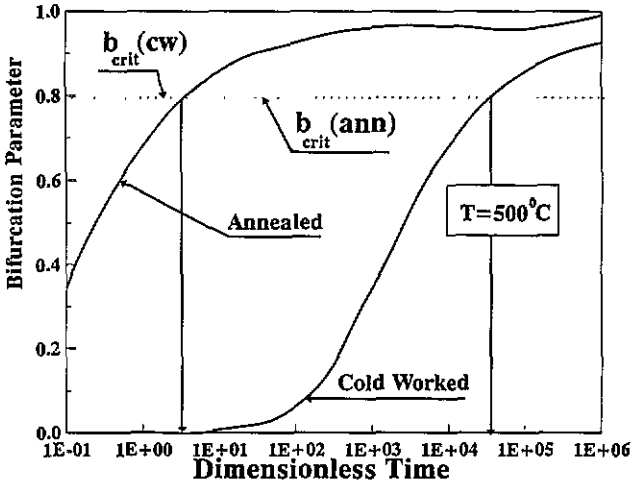

Figure 5. Evolution of the bifurcation parameter with irradiation dose for cold worked and annealed steels irradiated in typical low temperature conditions (i.e. $K = 10^{-3}$ dpa s^{-1} and $T = 500$ °C). The dashed lines represent the critical values of the bifurcation parameter.

ordered microstructures is achieved, even for cold worked steels, at small irradiation doses as shown in figure 5.

Form equations (5) and (6), one can find an expression for the bifurcation parameter at any dose. After a relatively short transient, both types of loops will grow with the same $\sqrt{\tau}$ time dependence. Hence, it is interesting to see that the bifurcation parameter, $b(\tau)$, tends to a constant value, given by:

$$b = \epsilon P/(\epsilon P + P\Delta B + \Delta) = \epsilon/\epsilon'. \tag{18}$$

This very interesting result implies that the distance from the critical value, b_c, is

fixed by material and irradiation variables, and that the nature of the dissipative periodic microstructure is determined after the start of irradiation. The reduced bifurcation parameter, $\zeta = (b - b_c)/b_c$, is also a fixed number, and is given by

$$\zeta = \left[(\epsilon/\epsilon' - 1) + \left(1 - \sqrt{\epsilon/B}\right)^2\right]/2\epsilon/B. \tag{19}$$

It will be shown in the next section that this condition does not mean that once a dissipative structure has formed (e.g., rolls, BCC, etc), it will remain unchanged with dose. In fact, the effects of increasing the dose will be manifest in the non-linearities of the system.

4. Stability analysis in the weakly non-linear regime

It is clear from the signs of the linear evolution matrix eigenvalues that the dislocation loops are subject to spatial instabilities, since there is at least one eigenvalue that can turn positive leading to growth in spatial fluctuations. The presence of non-linear reaction terms in (1) can be shown to saturate the growth of fluctuations. In this section we will extend our analysis to the weakly non-linear regime in order to describe the symmetries associated with the evolution of the microstructures.

We will again simplify the problem by acknowledging the stabilizing role of recombination [20, 21]. We will also adiabatically eliminate the time-dependence of point defect equations. Furthermore, in the vacancy-loop dominated regime, the dynamics is given by the evolution of the vacancy-loop density, all the other defect densities being slaved to it. With these simplifications, we take the Fourier transform of the vacancy-loop equation (equation (3)), which gives:

$$\tau_V \dot{\tilde{\rho}}_{V,q} = \epsilon P \delta_{q,0} - \int \mathrm{d}k\ \tilde{\rho}_{V,q-k}\left\{\mu(1 + \Delta B)\tilde{x}_{i,k} - (\tilde{x}_v - \tilde{x}_{vL})_k\right\}. \tag{20}$$

The symbol $\sim$ is used for variables in the Fourier space, and $\delta_{q,0}$ is the Dirac delta function. Notice that we used the convolution property of the Fourier transform to derive equation (20). Now, inserting (8) and (9) into (20), we obtain

$$\tau_V \dot{\tilde{\rho}}_{V,q} = \epsilon P \delta_{q,0} - \int \mathrm{d}k\ \tilde{\rho}_{V,q-k}\left\{\frac{\epsilon P + \Delta}{A_0}\delta_{k,0} - \int_{k' \neq 0} \mathrm{d}k' \left(\frac{\mu(1 + \Delta B)\delta\tilde{x}_{i,k-k'}}{A_{Ik}} - \frac{\delta\tilde{x}_{v,k-k'}}{A_{Vk}}\right)\tilde{\rho}_{V,k'}\right\}. \tag{21}$$

In equation (21), the first term on the right-hand side is a constant and corresponds to the homogeneous solution of the vacancy-loop concentration, the second term is a single integral over all wave vectors, k, and the third term is a double integral over k and k'. Let us now consider this double integral separately. Denoting the integral by I, and utilizing equations (8) and (9) again, we obtain:

$$I = -\int \mathrm{d}k \int_{k' \neq 0} \mathrm{d}k'\ \tilde{\rho}_{V,q-k}\left\{\left[\frac{\mu(1 + \Delta B)\tilde{x}_{i,0}}{A_{Ik}} - \frac{(\tilde{x}_v - \tilde{x}_{vL})_0}{A_{Vk}}\right]\delta_{k-k',0} + \dots\right\}\tilde{\rho}_{Vk}. \tag{22}$$

Rewriting this equation in ascending powers of $\tilde{\rho}_V$, and noting that when $k' = k$, the first term is obtained, we get:

$$I = -\int_{k\neq 0} \mathrm{d}k\tilde{\rho}_{v,q-k}\left\{\left[\frac{\mu(1+\Delta B)\tilde{x}_{i,0}}{A_{Ik}} - \frac{(\tilde{x}_v - \tilde{x}_{vL})_0}{A_{Vk}}\right]\tilde{\rho}_{v,k} + \ldots\right\} \tag{23}$$

$$= -\int_{k\neq 0} \mathrm{d}k\tilde{\rho}_{v,q-k}\left(\frac{P(1+\Delta B)}{A_{Ik}A_0} - \frac{\bar{P}}{A_{Vk}A_0}\right)\tilde{\rho}_{v,k} + \ldots \tag{24}$$

$$= -\tilde{\rho}_{V,0}\left(P(1+\Delta B)A_{Iq}A_0 - \bar{P}/A_{Vq}A_0\right)\tilde{\rho}_{V,q}$$

$$-\int_{\substack{k\neq 0\\(q-k)\neq 0}} \mathrm{d}k\left(\frac{P(1+\Delta B)}{A_{Ik}A_0} - \frac{\bar{P}}{A_{Vk}A_0}\right)\tilde{\rho}_{v,q-k}\tilde{\rho}_{v,k} + \ldots. \tag{25}$$

The form of the integral, I given by equation (25), together with equation (21) will now allow us to extract terms which contain various powers of $\tilde{\rho}_{v,q}$. The linear part of the evolution equation (21) may then be written as:

$$\tau_V\dot{\tilde{\rho}}_{V,q} = -\left(\epsilon P + \Delta/A_0\right)\tilde{\rho}_{V,q} + \tilde{\rho}_{V,0}\left[P(1+\Delta B)/A_{Iq}A_0 - \bar{P}/A_{Vq}A_0\right]\tilde{\rho}_{V,q}. \tag{26}$$

The quadratic term can be obtained by taking the first integral in the series represented by equation (25), i.e.

$$\int_{\substack{k\neq 0\\(q-k)\neq 0}} \mathrm{d}k\left(\frac{P(1+\Delta B)}{A_{Ik}A_0} - \frac{\bar{P}}{A_{Vk}A_0}\right)\tilde{\rho}_{V,q-k}\tilde{\rho}_{Vk}. \tag{27}$$

The cubic term is similarly obtained by going back to equation (22), and substituting terms from equations (8) which are only first order in $\tilde{\rho}_{V,k'}$. This cubic term is then given by:

$$-\int \mathrm{d}k\int \mathrm{d}k'\left[\frac{P(1+\Delta B)}{A_{Ik}A_{Ik'}A_0} - \frac{\bar{P}}{A_{Vk}A_{Vk'}A_0}\right]\tilde{\rho}_{V,q-k-k'}\tilde{\rho}_{V,k}\tilde{\rho}_{V,k'}. \tag{28}$$

We now introduce a definition of the order parameter, σ, which will describe the deviation of the spatial fluctuation from the uniform density.

$$\sigma_q = \delta\tilde{\rho}_{V,q} = \left(\tilde{\rho^*}_{V,q} - \rho_V^0\right)/\rho_V^0. \tag{29}$$

An evolution equation for σ_q can be written if we use the definition given by (29) and equations (26)–(28).

$$\tau_V\dot{\sigma}_q = -\left\{\left(\epsilon P + \Delta/A_0\right)/\rho_V^0 - \left[P(1+\Delta B)/A_{Iq}A_0 - \bar{P}/A_{Vq}A_0\right]\rho_V^0\right\}\sigma_q$$

$$+\int \mathrm{d}k\left[\frac{P(1+\Delta B)}{A_{Ik}A_0} - \frac{\bar{P}}{A_{Vk}A_0}\right]\rho_V^0\sigma_{q-k}\sigma_k \tag{30}$$

$$-\int \mathrm{d}k\int \mathrm{d}k'\left[\frac{P(1+\Delta B)}{A_{Ik}A_{Ik'}A_0} - \frac{\bar{P}}{A_{Vk}A_{Vk'}A_0}\right](\rho_V^0)^2\sigma_{q-k-k'}\sigma_k\sigma_k' + \ldots.$$

We notice from equation (30) that the coefficients in the linear and quadratic terms of the order parameter evolution equation can be positive and therefore can lead to an exponential

growth of small spatial fluctuations. The coefficient in the cubic term, however, is negative and will saturate the spatial instability. It can be shown that, at the critical wave-vector, q_c, the coefficient of the higher order non-linear term associated with $(\sigma_{q_c})^n$ assumes the form:

$$(-1)^n(\rho_V^0)^{n-1}/A_0\big[P(1+\Delta B)/A_{Iq_c}^{n-1} - \bar{P}/A_{Iq_c}^{n-1}\big]. \tag{31}$$

Hence, the contributions of higher order terms to the order parameter evolution equation (30) diminish and since the coefficients of odd powers of σ are negative, we need not consider terms of order above $n = 3$.

Close to the instability point, we may express the linear term as (see Appendix C for details):

$$(1/\tilde{\tau})\big[(b-b_c)/b_c - \zeta_0^2(q^2-q_c^2)^2\big]\sigma_q \tag{32}$$

where the bifurcation parameter, b, is given by

$$b = \rho_V^0/(1+\rho_V^0+\rho_I^0)$$

and its threshold value, b_c is given in Appendix B. The threshold wavevector, q_c, is also given in Appendix B. τ_0 and ζ_0 are constants.

In this regime, the weakly non-linear equation for σ_q may then be written as:

$$\begin{aligned}\tau_0\dot{\sigma}_q = &\left[\frac{b-b_c}{b_c} - \zeta_0^2(q^2-q_c^2)^2\right]\sigma_q + v\int \mathrm{d}k\,\sigma_{q-k}\sigma_k \\ &- u\int \mathrm{d}k\int \mathrm{d}k'\,\sigma_{q-k-k'}\sigma_k\sigma_{k'} + \ldots\end{aligned} \tag{33}$$

where

$$\begin{aligned}\tau_0 &= \tau_v\tilde{\tau} = \tau_v(\epsilon'+2B)^2/\epsilon PB(\epsilon'+B) \\ v &= \big(P(1+\Delta B)/A_{Iq_c}A_0 - \bar{P}/A_{Vq_c}A_0\big)\rho_V^0 = \big(\epsilon P/\rho_V^0\big)\tilde{\tau} \\ u &= \big(P(1+\Delta B)/A_{Iq_c}^2A_0 - \bar{P}/A_{Vq_c}^2A_0\big)(\rho_V^0)^2 = \big(\epsilon Pb_c/\rho_V^0\big)\tilde{\tau}.\end{aligned} \tag{34}$$

In real space one has:

$$\tau_0\dot{\sigma} = \Big[\big(b-b_c\big)/b_c - \zeta_0^2(\nabla^2+q_c^2)^2\Big]\sigma + v\sigma^2 - u\sigma^3. \tag{35}$$

When ρ_I^0 cannot be neglected versus ρ_V^0, the kinetic equations for the loop densities are not decoupled. The order-parameter-like variable is, in this case, a linear combination of $\delta\rho_{V,q}^0$ and $\delta\rho_{I,q}^0$ which is proportional to the eigenvector of the linear evolution matrix associated with the vanishing eigenvalue which induces the instability. After diagonalization of the linear part of the dynamics, the usual adiabatic elimination procedure of the stable modes may be performed. The resulting evolution equation for the order parameter has then the same structure as (33), the actual values of the coefficients being only modified. For the sake of simplicity, we will restrict our analysis to the vacancy-loops dominated case. This condition corresponds to experimental situations where $(\Delta B + \Delta/P)/\epsilon$ is small, since

$$\rho_I^0/\rho_V^0 = \big[(\epsilon'-\epsilon)/\epsilon\big]\rho_I^0/(1+\rho_I^0). \tag{36}$$

The condition is easily achieved at temperatures below half of the melting point. Thermal emission would be negligible under these circumstances. Also ΔB is usually small, and of the order of a few percent [22].

We thus recover the slow mode dynamics analysed in [12] but in the present case the coefficients of the linear terms decrease with time, since they are inversely proportional to ρ_V^0. Hence, and in the quasi-static approximation, the stability limits of the different structures evolve in time. This is because they are proportional to $v^2/u \propto 1/\rho_V^0$, while their amplitudes increase and are proportional to $\sqrt{\rho_V^0}$ well above threshold.

Let us recall that for the dynamics defined by equation (33), the stability range for critical BCC microstructures is given by $-v^2/33u < (b - b_c)/b_c < 3v^2/u$, while wall structures are only stable for $v^2/u < (b - b_c)/b_c$ [12]. However, as discussed in [23], since this dynamics is variational, BCC microstructures should be selected in the range given by $\zeta_1 = -8v^2/297u < \zeta = (b - b_c)/b_c < \zeta_2 = 3v^2/u$, while critical wall structures should be selected for $\zeta_2 = 3v^2/u < \zeta = (b - b_c)/b_c$. The corresponding bifurcation diagram is schematically shown in figure 6 for a particular dose. Since the dose is continuously increasing, and since ξ tends to a constant value at high doses, while v^2/u decreases and finally tends to zero, the following scenarios should be observable.

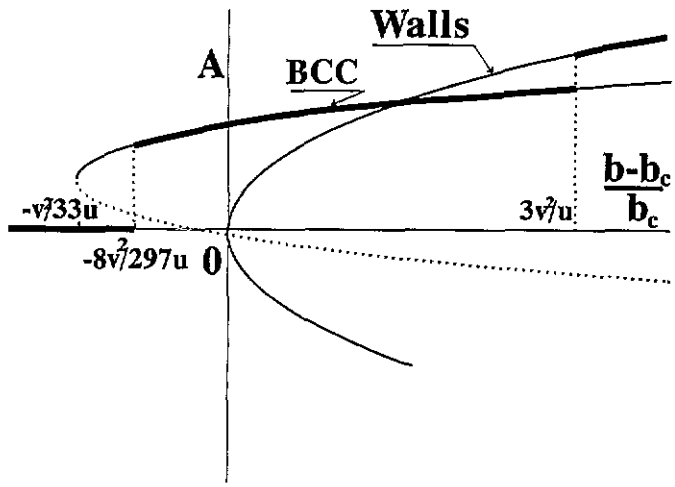

Figure 6. Bifurcation diagram for the stationary solutions of equation (33). Solid lines represent stable states, dashed lines represent unstable states, and heavy lines correspond to the minimum of the associated Lyapounov functional.

(i) When $(b - b_c)/b_c$ tends to a positive value, BCC structures may appear in the early stages of the irradiation process but the final state corresponds to wall structures. This should be the case for annealed steel in reactor or accelerator conditions. The reactor conditions are illustrated in figure 7 for 500 °C. In this case, one observes a succession of domains where different types of microstructures may be selected. In the first one, both BCC and uniform loop distributions are stable; then appears a domain where only uniform distributions are stable followed by domains where BCC and wall structures are successively selected.

(ii) When $(b - b_c)/b_c$ tends to a negative value, the final state corresponds to uniform-loop distributions, but BCC microstructures may still appear as transients. In this case no

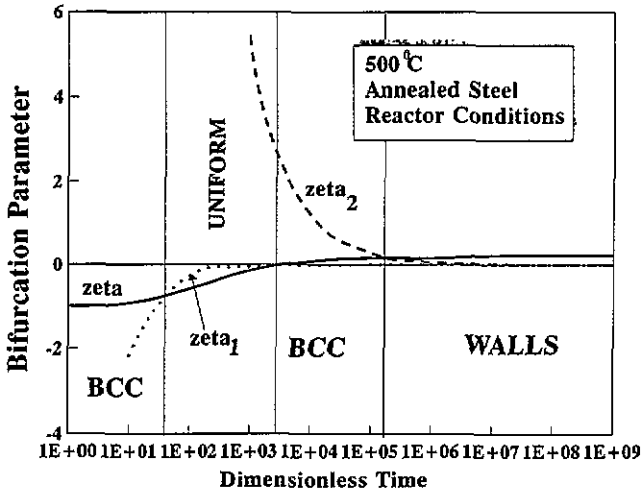

Figure 7. Pattern selection for annealed steel in typical reactor conditions (i.e. $K = 10^{-6}$ dpa s^{-1} and $T = 500$ °C) as a function of time in the quasi-static approximation. BCC structures are selected when $\zeta_1 < \zeta < \zeta_2$ while wall structures are selected for $\zeta_2 < \zeta$. No patterning can occur for $\zeta < \zeta_1$.

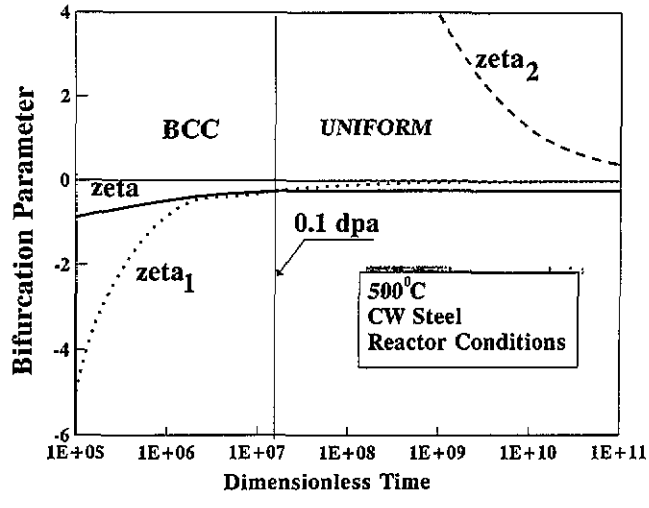

Figure 8. Pattern selection for cold worked steel in typical reactor conditions ($K = 10^{-6}$ dpa s^{-1} and $T = 500$ °C) as a function of time in the quasi-static approximation. BCC structures are selected when $\zeta_1 < \zeta < 0$ while no patterning can occur for $\zeta < \zeta_1$.

wall structures can be formed. This should, for example, be the case for cold worked steel in reactor conditions at 500 °C as illustrated in figure 8.

Hence, one sees that 3D BCC microstructures should only appear as transient states while the final state should correspond to uniform distributions or plane wall structures.

5. Effects of point defect diffusion anisotropy

In the preceding section, we discussed the formation and evolution of defect microstructures in irradiated metals in an isotropic medium, i.e. when the diffusion coefficients of point defects are isotropic. Let us analyse here what happens when this is not the case. The experimentally relevant case corresponds to anisotropic interstitial mobilities, and, on assuming that this only affects the diffusive part of the interstitial evolution, the dynamical model (1) has then to be rewritten as:

$$\begin{aligned}
\partial_t c_i &= K - \alpha c_i c_v + \nabla_m D_i^{(mn)} \nabla_n c_i - D_i c_i (Z_{iN}\rho_N + Z_{iV}\rho_V + Z_{iI}\rho_I) \\
\partial_t c_v &= K(1-\epsilon) - \alpha c_i c_v + D_v \nabla^2 c_v - D_v \big(Z_{vN}(c_v - \bar{c}_{vN})\rho_N \\
&\qquad + Z_{vV}(c_v - \bar{c}_{vV})\rho_V + Z_{vI}(c_v - \bar{c}_{vI})\rho_I\big) \\
\partial_t \rho_I &= (2\pi N/|b|)\Big(D_i Z_{iI} c_i - D_v Z_{vI}\big(c_v - \bar{c}_{vI}\big)\Big) \\
\partial_t \rho_v &= \big(1/|b| r_V^0\big)\big[\epsilon K - \rho_v \big(D_i Z_{iV} c_i - D_v Z_{vV}\big(c_v - \bar{c}_{vV}\big)\big]
\end{aligned} \tag{37}$$

with $m, n = x, y, z$.

When interstitials have higher mobility in planes perpendicular to a well-defined direction, say in planes parallel to the x0y plane and perpendicular to the 0z direction, $\nabla_m D_i^{(mn)} \nabla_n$ becomes $D_{i\parallel}(\nabla_x^2 + \nabla_y^2) + D_{i\perp}\nabla_z^2$ or $D_i(\nabla^2 + \beta\nabla_\perp^2)$ with $D_i = D_{i\perp}$ and $\beta > 1$. When the interstitials have a higher mobility in a well-defined direction, say 0z, $\nabla_m D_i^{(mn)} \nabla_n$ becomes $D_{i\parallel}\nabla_z^2 + D_{i\perp}(\nabla_x^2 + \nabla_y^2)$ or $D_i(\nabla^2 + \beta\nabla_z^2)$, with $D_i = D_{i\perp}$ and $\beta > 1$.

Hence, on performing the linear stability analysis of uniform densities, the only modification that occurs in (14) is that A_{l_q} has to be replaced by its anisotropic counterpart $A_{l_q}^a = A_{l_q} + [\bar{D}_y/(1+B)](q^2 + \beta q_\perp^2 (\text{or } q_x^2))$, according to the type of anisotropy. The critical wave vector being the one which minimizes the threshold value of the bifurcation parameter, it is also the one which minimizes $A_{l_q}^2$, and the instability point is now defined by:

$$\begin{aligned}
b_c &= \left.\frac{\rho_V^0}{A_0}\right|_c = \left.\frac{\rho_V^0}{1 + \rho_V^0 + \rho_I^0}\right|_c \simeq \frac{1}{2}\left[\frac{\rho_I^0}{\rho_V^0} + \sqrt{\left(\frac{\rho_I^0}{\rho_V^0}\right)} + \frac{4\epsilon B}{(\epsilon' + B)^2}\right] \\
q_c^2 &= \rho_{V^c}^0 \sqrt{1+B}/2\sqrt{\epsilon/B}
\end{aligned} \tag{38}$$

with $q_c = q_c \mathbf{1}_z$ for easy-plane anisotropy and $q_c = q_c \mathbf{1}_\perp$ for easy-axis anisotropy.

The linear growth rate of the order-parameter-like variable is now given by (cf Appendix C):

$$\big(b - b_c\big)/b_c - \big(q_c^2 + \nabla^2\big)^2 + \kappa\nabla_z^2$$

in the easy-axis case, and by

$$\big(b - b_c\big)/b_c - \big(q_c^2 + \nabla^2\big)^2 + \kappa\nabla_\perp^2$$

in the easy-plane case.

Near the instability point, the weakly non-linear approximation for the dynamics of defect populations may be worked out as above, and one obtains the following evolution equation for the order parameter-like variable in the easy-plane case:

$$\tau_0 \partial_t \sigma(r,t) = \big[\big(b - b_c\big)/b_c - \big(q_c^2 + \nabla^2\big)^2 + \kappa\nabla_\perp^2\big]\sigma(r,t) + v\sigma^2(r,t) - u\sigma^3(r,t) \tag{39}$$

where $\nabla^2 = \nabla_x^2 + \nabla_y^2 + \nabla_z^2$ and $\nabla_\perp^2 = \nabla_x^2 + \nabla_y^2$.

From this kinetic equation, one can derive the amplitude equations for the various patterns which may appear beyond the bifurcation point. It has to be noted that the orientational degeneracy of the isotropic systems is lifted since the first mode to bifurcate has his wavevector parallel to the z-axis and corresponds to a planar wall structure with planes parallel to the planes of high interstitial mobility. The vacancy-loop density in this case is defined by:

$$\sigma(r,t) = A(r,t)e^{iq_c z} + \bar{A}(r,t)e^{-iq_c z}$$

where A are slowly evolving functions on space scales much larger than $2\pi q_c^{-1}$ and satisfy the following amplitude equation:

$$\tau_0 \partial_t A = \left[(b - b_c)/b_c + 4q_c^2 \nabla_z^2 + \kappa \nabla_\perp^2\right] A - 3uA|A|^2. \tag{40}$$

One thus recovers here the usual amplitude equation for wall structures in anisotropic media [24].

Since the quadratic non-linearities of the kinetic equation (39) still couple this mode with modes having the same wavenumber but which make $2\pi/3$ angles with it, one has to test the stability of the planar wall structure versus these modes. The corresponding set of uniform amplitude equations is:

$$\begin{aligned}
\tau_0 \partial_t A &= A + v\bar{B}\bar{C} - 3uA(|A|^2 + 2|B|^2 + 2|C|^2) \\
\tau_0 \partial_t B &= \left[(b - b_c)/b_c - \tfrac{3}{4}q_c^2\kappa\right] B + v\bar{A}\bar{C} - 3uB(|B|^2 + 2|A|^2 + 2|C|^2) \\
\tau_0 \partial_t C &= \left[(b - b_c)/b_c - \tfrac{3}{4}q_c^2\kappa\right] C + v\bar{A}\bar{B} - 3uC(|C|^2 + 2|A|^2 + 2|B|^2)
\end{aligned} \tag{41}$$

where B and C are respectively the amplitudes of modes of wavevectors $q = -(q_c/2)\mathbf{1}_z + (\sqrt{3q_c}/2)\mathbf{1}_\perp$ and $q = -(q_c/2)\mathbf{1}_z - (\sqrt{3q_c}/2)\mathbf{1}_\perp$. $\mathbf{1}$ is a unit vector in the axial direction, and $\mathbf{1}_\perp$ is a unit vector on the perpendicular plane.

The linear evolution of the modes B and C in the presence of a steady wall structure of amplitude $\sqrt{(b - b_c)/b_c}$ is thus given by

$$\begin{aligned}
\tau_0 \partial_t B &= -\left[(b - b_c)/b_c + \tfrac{3}{4}q_c^2\kappa\right] B + v\sqrt{(b - b_c)/3ub_c}\, C \\
\tau_0 \partial_t C &= -\left[(b - b_c)/b_c + \tfrac{3}{4}q_c^2\kappa\right] C + v\sqrt{(b - b_c)/3ub_c}\, B
\end{aligned} \tag{42}$$

and the eigenvalues of the corresponding evolution matrix are

$$\omega = (b - b_c)/b_c - \tfrac{3}{4}q_c^2\kappa \pm v\sqrt{(b - b_c)/3ub_c}. \tag{43}$$

Hence, the planar wall structure is always stable when $\kappa > v^2/9uq_c^2$. Let us note that the time dependence of the variables involved in this condition is such that it only depends on materials parameters at high doses. If this condition is not satisfied, there is a window in $\zeta = (b - b_c)/b_c$, defined by

$$\begin{aligned}
\tfrac{1}{2}\left[v/3u - \sqrt{v^2/3u - 3q_c^2\kappa(\gamma - 1)}\right] &< \sqrt{(b - b_c)/b_c} \\
&< \tfrac{1}{2}\left[v/3u + \sqrt{v^2/3u - 3q_c^2\kappa(\gamma - 1)}\right]
\end{aligned} \tag{44}$$

where the wall structure is unstable. In this regime anisotropic 3D structures may be expected but, since this window shrinks with increasing dose, and the final structure should consist in planes parallel to the planes of high interstitial mobility, as is experimentally observed [27].

In the easy axis case, i.e. when the interstitial mobility is maximum in one direction (e.g. 0z), the discussion made above may easily be transposed. There is in this case a circle of critical wavevectors which lies in the plane perpendicular to the direction of high mobility and the weakly non-linear dynamics may be written as:

$$\tau_0 \partial_t \sigma(r,t) = \left[\left(b - b_c\right)/b_c - \left(q_c^2 + \nabla^2\right)^2 + \kappa \nabla_x^2\right]\sigma(r,t) + v\sigma^2(r,t) - u\sigma^3(r,t) \qquad (45)$$

where $\nabla^2 = \nabla_x^2 + \nabla_y^2 + \nabla_z^2$. In this case, the first structure to be expected is a rodlike hexagonal structure with the rods parallel to the z direction. On increasing the constraint, as in the other cases discussed so far, this structure should become unstable and lead to a planar wall structure with walls parallel to the z-axis.

6. Experimental evidence

Experimental observations of periodic 3D microstructures have clearly shown the existence of clusters of cubic symmetry [28,29], defect walls [30,31], as well as anisotropic arrangements of planar aggregates of defects [32–34]. It is experimentally verified that cascade production is necessary for the formation of 3D periodic microstructures. Irradiation with electrons (no cascade) does not produce ordered arrays of defect clusters [11]. The only alignments of stacking fault tetrahedra (SFT) occur along (100) directions in Cu [35,36] and Au [37]. However, these alignments were not observed in 3D, nor did they extend well into the irradiated area. Periodic walls were also not observed when gas atoms, such as H or He, were pre-implanted [38].

The temporal evolution of the spatial evolution of 3D periodic arrangements of defect clusters has been documented recently [11]. Only in a few cases were defect clusters of cubic symmetry observed [28]. At low doses, spatial fluctuations of cluster densities were generally observed. However, blocks or agglomerates of defect clusters along cubic axes were observed to disappear at higher doses in favour of planar walls parallel to {100} matrix planes in Cu and Ni. Up to a dose of 4 dpa, no competing arrangement of higher stability than planar walls were observed.

7. Conclusions

It has been shown that the coupling between reaction and transport induces pattern-forming instabilities in defect distributions in irradiated crystalline materials. For example, uniform distributions of point defects such as interstitials and vacancies in irradiated materials may become unstable and lead to the precipitation of solid solutions, to the nucleation of voids and of void lattices. In this framework, it is shown that vacancy-loop ordering occurs under very general conditions in irradiated metals and alloys. It mainly results from a Turing-like instability induced by the different mobilities and bias in the migration of point defects to line defects such as dislocation loops or network dislocations. According to the generic properties of such pattern forming instability, structures with different symmetries, such as BCC lattices or wall structures, may be simultaneously stable in well-defined parameter

ranges. However, at sufficiently high values of the bifurcation parameter, the only stable structure corresponds to planar arrays.

Here, one has to take into account that the microstructure is continuously evolving. In such cases, our analysis predicts that, in the case of stainless steel (or nickel) irradiated under typical reactor conditions, the effective bifurcation parameter continuously increases with time or irradiation dose. Hence, after an initial phase where loop clustering should occur in the form of BCC lattices, the system evolves towards a uniform state followed by a transient BCC structure and finally reaches a planar wall structure, even for isotropic defect mobilities. These structures could then be in non-parallel orientations, i.e. with a structure different from the structure of the host lattice. This behaviour, which seems consistent with many experimental observations, also occurs under accelerator conditions, particularly for an initially annealed microstructure. In the case of anisotropic interstitial diffusion, planar structures should also be the rule, but in this case, the orientation of the walls are determined by the diffusion anisotropy. For heavily cold worked initial microstructures, the bifurcation parameter cannot reach the instability threshold. However, since BCC structures may appear subcritically, 3D loop clustering could occur transitorily, but the final defect distributions should be uniform.

Hence, since the symmetry of the defect structures is a crucial issue in irradiated materials, the present discussion shows that a careful study of the post-bifurcation regime is needed to test the relevance of particular kinetic models to the interpretation of experimental observations. Furthermore, we believe that a coherent description of materials instabilities that induce the spatio-temporal organization of defect populations will hopefully lead to a deeper understanding of the behaviour of irradiated materials. Indeed, due to the strong non-equilibrium conditions under which irradiation induced defect patterning occurs, classical mechanical or thermodynamical considerations are not sufficient to interpret these phenomena and we need to study them in the framework of non-linear dynamics and instability theory. In particular, we showed that, despite the huge complexity of defect dynamics, even in the case of phenomenological models, valuable information can be obtained via the reduced dynamics near instability points leading to a realistic description of the pattern selection and stability properties in the post-bifurcation regime. Hence, we believe that by the combination of the results of bifurcation analysis, amplitude equation formalism and numerical simulations, significant progress may be expected in understanding and prediction of the effects of materials instabilities on the macroscopic behaviour of driven or degrading solids.

Acknowledgments

Financial assistance through a collaborative research grant of the NATO Scientific Affairs Division (890489) is gratefully acknowledged.

Appendix A. Defect dynamics under irradiation

The dynamics of free and clustered defects under irradiation involves the solution of hierarchical rate equations [25], or equivalently, coupled rate/Fokker–Plank equations [26]. However, since we are not interested in the evolution of the size distribution of clustered

defects, but rather in their spatial stability against fluctuations in point defect concentrations, we can simplify defect dynamics in the following set of equations:

$$\partial_t c_v = K(1-\epsilon) - \alpha c_i c_v - K_{v2} c_v c_{2i} - D_v\big[Z_{vN}\big(c_v - \bar{c}_{vN}\big)\rho N + Z_{vV}\big(c_v - \bar{c}_{vV}\big)\rho V + Z_{vI}\big(c_v - \bar{c}_{vI}\big)2bc_I\sqrt{\pi X}\big] + D_v\nabla^2 c_v \tag{A1}$$

$$\partial_t c_i = K - \alpha c_i c_v - D_i c_i\big(Z_{iN}\rho_N + Z_{iV}\rho_V + 2Z_{iI}bc_I\sqrt{\pi X}\big) + K_{V2}c_V c_{2i} + 2\delta c_{2i} - K_{11}c_i^2 - K_{12}c_i c_{2i} + D_i\nabla^2 c_i \tag{A2}$$

$$\partial_i c_{2i} = K_{11}c_i^2 - K_{12}c_i c_{2i} - 2\delta c_{2i} - 2K_{22}c_{2i}^2 - D_{2i}c_{2i}\big(Z_{2iN}\rho_N + Z_{2iV}\rho_V + 2Z_{2iI}bc_I\sqrt{\pi X}\big) + D_{2i}\nabla^2 c_{2i} \tag{A3}$$

$$\partial_t N = K_{12}c_i c_{2i} + 2K_{22}c_{2i}^2 \tag{A4}$$

$$\partial_t X = K(X)\big[D_i Z_{iI} c_i - D_v Z_{vI}\big(c_v - \bar{c}_{vI}\big)\big] - (X-3)\partial_t N/N. \tag{A5}$$

In the equations (A1)–(A5) the reaction rate constants between species a and b are represented by K_{ab}, and are mainly dependent on the diffusivity of the mobile species. Nucleation of interstitial clusters proceed homogeneously, at a critical size of two interstitial atoms. Solution of equations (A1)–(A4) results in the determination of the time-dependent interstitial loop concentration. However, the time scale for nucleation of interstitial clusters is very short (see [25]). This will greatly simplify the present model, where we can safely assume that the total number density of interstitial loops, N, is constant. Equation (A5) gives the growth rate of the average interstitial loop size, where X is used for the average number of atoms in a loop. On the basis of fast loop nucleation, the term $\partial_t N/N$ drops out. The bias factor $K(X)$ can be strongly size dependent for very small loops [22]. An average value, Z_{iI} will be used in our calculations. Equation (A5) then becomes:

$$\partial_t r = (1/|b|)\big[D_i Z_{iL} C_i - D_V Z_V L\big(C_V - \bar{C}_{VL}\big)\big]. \tag{A6}$$

Since $\rho_l = 2\pi r N$, we can finally write the following two equations for the dislocation density of clustered defects.

$$\partial_t \rho_I = (2\pi N/|b|)\big[D_i Z_{iL} C_i - D_V Z_V L\big(C_V - \bar{C}_{VL}\big)\big] \tag{A7}$$

$$\partial_t \rho_v = (1/|b|r_V^0)\big[\epsilon K - \rho_V\big(D_I Z_{IV} c_i - D_v Z_{vV}\big(c_v - \bar{c}_{vV}\big)\big)\big]. \tag{A8}$$

As a final approximation, the effects of nucleation on C_i and C_v will be neglected, which leads to the set of four equations, for free and clustered point defects, as given in section 2.

Appendix B. The eigenvalues of the linear evolution matrix

We present in this appendix a detailed derivation of the critical eigenvalues in the quasi-static approximation. The evolution matrix equation which corresponds to (12) takes the form:

$$\partial_\tau \delta\bar{\rho}_q = \mathbf{M}_q \delta\bar{\rho}_q \tag{B1}$$

where $\delta\bar{\rho}_q$ is the density perturbation vector with components $\delta\rho_{v,q}$ and $\delta\rho_{I,q}$ for the Fourier wavevector q.

The evolution matrix $\mathbf{M}_q$ has the elements:

$$M_{11}^q = -\tau_V^{-1}\left(\epsilon P/\rho_V^0 - \rho_V^0\Gamma_{IV,q}\right) \tag{B2}$$

$$M_{12}^q = \tau_V^{-1}\rho_I^0\Gamma_{IV,q} \tag{B3}$$

$$M_{21}^q = -\tau_I^{-1}\left(\rho_v^0/\rho_I^0\right)\Gamma_{IV,q} \tag{B4}$$

$$M_{22}^q = -\tau_I^{-1}\left[\Gamma_{IV,q} + \left(\epsilon P + \Delta\right)/A_0\rho_i^0\right]. \tag{B5}$$

Now if we assume that the density perturbations follow solutions of the form:

$$\delta\rho_{Vq} = A_V e^{\omega t} \qquad \delta\rho_{Iq} = A_I e^{\omega t} \tag{B6}$$

where A_V and A_I are complex constants and ω is the frequency. Substituting (B2) in (B1), we obtain:

$$\mathbf{M}_q\begin{pmatrix} A_V \\ A_I \end{pmatrix} = \omega\begin{pmatrix} A_V \\ A_I \end{pmatrix} \tag{B7}$$

For a non-trivial solution of equation (B7), the determinant of the coefficients must vanish. This condition results in the dispersion relation:

$$\omega^2 - \omega\left(M_{11} + M_{22}\right) + \left(M_{11}M_{22} - M_{12}M_{21}\right) = 0. \tag{B8}$$

When the cross-terms ($M_{12}M_{21}$) in the matrix $\mathbf{M}_q$ are small, which is the case in the vacancy-loop dominated regime, the fluctuations in the loop densities $\delta\rho_{Vq}$, $\delta\rho_{Iq}$ are almost decoupled. Since this is not always attained, let us discuss the general case here. Note that a detailed investigation of the dispersion relation (B8) is given by Ghoniem and Abromeit [18].

Again, using the simplification that $Z_{i,} \cong 1$, the uniform distributions are unstable when $M_{12}M_{21} \geqslant M_{11}M_{22}$, i.e.

$$\epsilon P/\rho_v^0 \leqslant \rho_v^0\Gamma_{IV,q}(\epsilon P + \Delta)/(\epsilon P + \Delta + \rho_I^0 A_0\Gamma_{IV,q}) \tag{B9}$$

or

$$\Gamma_{IV,q}\left(1 - \left[\rho_I^0 A_0/(\rho_v^0)^2\right]\epsilon P/(\epsilon P + \Delta)\right) \geqslant \epsilon P/(\rho_v^0)^2 \tag{B10}$$

and the critical wavevector q_c is the wavevector which minimizes this threshold condition. It is thus defined by the condition:

$$\frac{P(1+\Delta B)}{1+B}\left(\frac{1}{A_0 + q_c^2 D_V/(1+B)}\right)^2 = \frac{\bar{P}}{(A_0 + q_c^2 D_V)^2}. \tag{B11}$$

substituting (B11) into (B9), we can obtain the following condition for the threshold wavevector q_c:

$$\frac{\epsilon P}{\rho_v^0} - \left(\frac{\rho_v^0 P(1+\Delta B)B}{1+B}\right)\left(\frac{1}{A_0 + q_c^2 D_V/(1+B)}\right)^2\left(1 - \frac{\rho_I^0 A_0}{(\rho_v^0)^2}\frac{\epsilon P}{\epsilon P + \Delta}\right) = 0. \tag{B12}$$

At this point, we introduce a bifurcation parameter, $b = \rho_v^0/A_0$, which controls the dispersion relationship. For values of b less than a critical quantity, b_c, the system is always stable against infinitesimal spatial fluctuations. The solution of equations (B9) and (B12) gives the instability threshold which is defined by:

$$\left(\frac{\rho_v^0}{A_0}\bigg|_c\right)^2 - \frac{\rho_I^0}{\rho_v^0}\frac{\epsilon P}{\epsilon P + \Delta}\left(\frac{\rho_v^0}{A_0}\bigg|_c\right) \simeq \frac{4\epsilon B}{(B+\epsilon')^2} \tag{B13}$$

which gives

$$b_c = \frac{\rho_v^0}{A_0}\bigg|_c = \frac{\rho_v^0}{1+\rho_v^0+\rho_I^0}\bigg|_c \simeq \frac{1}{2}\left[\frac{\rho_I^0}{\rho_v^0} + \sqrt{\left(\frac{\rho_I^0}{\rho_v^0}\right)^2 + \frac{4\epsilon B}{(\epsilon'+B)^2}}\right] \tag{B14}$$

and

$$q_c^2 \bar{D}_v = \frac{A_0 B\sqrt{1+B}}{\epsilon'+B} = \frac{\rho_{vc}^0\sqrt{1+B}}{2\sqrt{\epsilon/b}} \tag{B15}$$

where $\epsilon' + \Delta B + \Delta/P$.

It is interesting to note that in the vacancy-loop dominated regime (i.e. when $\rho_I^0/\rho_V^0 \ll 1$), equations (B9) and (B13) may be written as

$$(\rho_v^0)^2 \Gamma_{IV,q} \geqslant \epsilon P \tag{B16}$$

and

$$(\rho_v^0/A_0)\Big|_c \simeq 2\sqrt{\epsilon B}/(\epsilon'+B). \tag{B17}$$

These equations are equivalently obtained by neglecting the off-diagonal elements of the linear evolution matrix. In this case, the evolution of the loop densities may be decoupled at the leading order in ρ_I^0/ρ_V^0.

As discussed in section 3, the actual value of the bifurcation parameter tends to a constant ($b \to \epsilon/\epsilon'$) and the condition for instability is only related to the value of materials parameters and becomes

$$\epsilon/\epsilon' > 2\sqrt{\epsilon B}/(\epsilon'+B) \tag{B18}$$

which is equivalent to (for $\Delta/P \ll \Delta B$)

$$B > \epsilon(1+\Delta B/\epsilon)\left[1 + 2\Delta B/\epsilon + \sqrt{(\Delta B/\epsilon)(1+\Delta B/\epsilon)}\right]$$

or

$$B < \epsilon(1+\Delta B/\epsilon)\left[1 + 2\Delta B/\epsilon - \sqrt{(\Delta B/\epsilon)(1+\Delta B/\epsilon)}\right]. \tag{B19}$$

It is also worth noting that the preferred wave number q_c increases with time since it is proportional to A_0 (cf (B15)).

Appendix C. The slow mode dynamics near threshold

Close to threshold, the linear growth rate of the order-parameter-like variable σ_q may be expanded in powers of $(b - b_c/b_c$ and $(q^2 - q_c^2)$. At the leading order, one obtains

$$\left(\frac{P(1+\Delta B)}{A_{Iq}A_0} - \frac{\tilde{P}}{A_{V_q}A_0}\right)\rho_v^0 - \frac{(\epsilon P + \Delta/A_0)}{\rho_v^0} = \frac{1}{\tilde{\tau}}\left[\frac{b-b_c}{b_c} - \zeta_0^2\left(q^2 - q_c^2\right)^2\right]. \tag{C1}$$

The coefficients τ and ζ_0^2 are obtained from the threshold conditions (B14) and (B15) and are found to be

$$\frac{1}{\tilde{\tau}} = \frac{A_0^2}{A_{Iq_c}}\left(\epsilon' + \frac{B}{\sqrt{1+B}}\right)P \simeq \frac{8\epsilon P B(\epsilon' + B)}{(\epsilon' + 2B)^2} \tag{C2}$$

which is constant in time, and

$$\zeta_0^2 = \left[\epsilon(\epsilon' + B)/8B(\epsilon' + 2B)\right]\left(\tilde{D}_v/A_0\right)^2 \tag{C3}$$

which decreases with time. Hence the band of wave numbers allowed for the spatial patterns increases with time. The increase in q_c with time would result in a shorter preferred wavelength of the organized periodic loop structure. In addition, since the band of wavelengths allowed for the loop structures, imperfections and a distribution of wavelengths are expected to develop.

At the leading order in $(b - b_c)/b_c$ and $(q^2 - q_c^2)$, one only needs to consider the values of the non-linear coefficients at b_c and q_c. Using the threshold conditions (B11) and (B17) one finds:

$$\left(\frac{P(1+\Delta B)}{A_{Iq_c}} - \frac{\tilde{P}}{A_{Vq_c}A_0}\right)\rho_v^0 = \frac{(\epsilon P + \Delta/A_0)}{\rho_v^0} \tag{C4}$$

and

$$\left(P(1+\Delta B)/A_{Iq_c}^2 - \tilde{P}/A_{Vq_c}^2 A_0\right)\left(\rho_v^0\right)^2 = (\epsilon P + \Delta/A_0)b_c/\rho_v^0 \tag{C5}$$

which leads to (33).

In the anisotropic case, since $A_{Iq}^a = A_{Iq} + [\tilde{D}_v/(1+B)](q^2 + \beta q_\perp^2 (\text{or } q_z^2))$, the linear growth rate of the order-parameter-like variable is given, in the easy plane case, by:

$$\begin{aligned}
&\left(P(1+\Delta B)/A_{Iq}^a A_0 - \tilde{P}/A_{Vq}A_0\right)\rho_v^0 - (\epsilon P + \Delta/A_0)/\rho_v^0 \\
&\quad = \frac{1}{\tilde{\tau}}\left[(b-b_c)/b_c - \zeta_0^2\left(q^2 - q_c^2\right)^2\right] \\
&\qquad - \left(1/A_{Iq}^a A_{Vq}\right)\left[(\epsilon P + \Delta/A_0)/\rho_v^0 + \tilde{P}\rho_v^0/A_0\right]\left([\beta/(1+B)]q_\perp^2\right) \\
&\quad = \frac{1}{\tilde{\tau}}\left[(b-b_c)/b_c - \zeta_0^2\left(q^2 - q_c^2\right)^2\right] - \kappa q_\perp^2
\end{aligned} \tag{C6}$$

with

$$\kappa = \left[\frac{(\epsilon P + \Delta/A_0)}{\rho_v^0} + \frac{\tilde{P}\rho_v^0}{A_0}\right]\frac{\beta}{(1+B)}\frac{\tilde{D}}{P(\epsilon' + B)A_0^2} \simeq \frac{\epsilon\beta}{\epsilon'(\epsilon' + B)}\frac{\tilde{D}_v}{(1+B)A_0^2}. \tag{C7}$$

One easily sees that, κ is algebraically decreasing in time as a result of its A_0^{-2} dependence.

References

[1] Evans J H 1971 *Nature* **229** 403; 1971 *Radiat. Eff.* **10** 55

[2] Kulcinski G L, Brimhall J L and Kissinger H E 1972 Production of voids in pure metals by high-energy heavy-ion bombardment *Proc. 1971 Int. Conf. Radiation-Induced Voids in Metals (Albany, NY, 1971)* USAEC, CONF-710601, NTIS p 465

[3] Wiffen F W 1972 The effect of alloying and purity on the formation and ordering of voids in BCC metals *Proc. 1971 Int. Conf. Radiation-Induced Voids in Metals (Albany, NY, 1971)* USAEC, CONF-710601, NTIS p 386

[4] Sass S and Eyre B L 1973 *Phil. Mag.* **27** 1447

[5] Johnson P B, Mazey D J and Evans J H 1983 *Radiat. Eff.* **78** 147

[6] Mazey D J and Evans J H 1986 *J. Nucl. Mater.* **138** 16

[7] Evans J H and Mazey D J 1985 *J. Phys. F: Met. Phys.* **15** L1; 1986 *J. Nucl. Mater.* **138** 176

[8] Jostons A and Farrell K 1972 *Radiat. Eff.* **15** 217

[9] Kulcinski G L and Brimhall J L 1973 *American Society for Testing and Materials Report* ASTM.STP 529 **227** p 258

[10] Steigler J O and Farrell K 1974 *Scr. Metall.* **8** 651

[11] Jager W, Ehrhart P and Schilling W 1988 *Nonlinear Phenomena in Materials Science* ed G Martin and L P Kubin (Aedermannsdorf: Transtech) p 279

[12] Walgraef D and Ghoniem N M 1989 *Phys. Rev.* B **39** 8867

[13] Murphy S M 1987 *Europhys. Lett.* **3** 1267

[14] Bullough R, Eyre B L and Krishan K 1975 *J. Nucl. Mater.* **44** 121

[15] Ghoniem N M and Kulcinski G L 1978 *Radiat. Eff.* **39** 47

[16] Newell A C 1974 *Lectures in Applied Mathematics* vol 15 ed M Kac (American Mathematical Society) p 157

[17] Haken H 1977 *Synergetics: an Introduction* 3rd edn (Berlin: Springer)

[18] Ghoniem N M and Abromeit C 1993 Effects of recombination and clustering on the stability of microstructures *J. Nucl. Mater.* to be submitted

[19] Jahvery R S and Hornsy C M 1983 *J. Fluid. Mech.* **144** 251

[20] Krishan K 980 *Nature* **287** 420

[21] Martin G 1975 *Phil. Mag.* **32** 615

[22] Wolfer W G and Ashkin M 1975 *J. Appl. Phys.* **46** 547

[23] Walgraef D, Dewel G and Borckmans P 1982 *Adv. Chem. Phys.* **49** 311

[24] Walgraef D and Schiller C 1987 *Physica* D **25** 423

[25] Ghoniem N M and Cho D O 1979 *Phys. Status Solidi* a **54** 171

[26] Ghoniem N M 1989 *Phys. Rev.* A **39** 11 810

[27] Hudson B 1964 *Phil. Mag.* **10** 949

[28] Kulcinski G L and Brimhall J L 1973 *American Society for Testing of Materials* ASTM-STP 529 p 258

[29] Stiegler J O and Farrell K 1974 *Scripta Met.* **8** 651

[30] Hulett Jr L D, Baldwin T O, Crump III J C and Young Jr F W 1968 *J. Appl. Phys.* **39** 3945

[31] Brimhall J L, Kulcinski G L, Kissinger H E and Mastel B 1971 *Radiat. Eff.* **9** 273

[32] Wilkes J and Clarke F J P 1964 *J. Nucl. Mater.* **14** 179

[33] Jostons A and Farrell K 1972 *Radiat. Eff.* **15** 217

[34] Koch E F and Lee D 1973 *Proc. 31st Ann. EMSA Meeting, Clartor's Pub. Division (Baton Rouge, 1973)* p 88

[35] Jager W and Urban K 1975 *Proc. Int. Conf. High Voltage Electron Microscopy (Toulouse, 1975)* ed B Jouffrey and P Favard (Paris: SFME) p 175

[36] Kiritani M 1975 Fundamental aspects of radiation damage in metals *US ERDA CONF-751006 (Oak Ridge, TN, 1975)* ed M T Robinson and R W Young Jr p 695

[37] Kubin L P, Rocher A, Rualt M O and Jouffrey B 1976 *Phil. Mag.* **33** 293

[38] Ehrhart P, Gaber A, Godalla A A, Jager W and Tsukuda N 1985 *J. Nucl. Mater.* **137** 73